Structural Durability & Health Monitoring

Tech Science Press

DOI: 10.32604/sdhm.2022.08886

ARTICLE

# Experimental Study on the Degradation of Bonding Behavior between Reinforcing Bars and Concrete after Corrosion and Fatigue Damage

**Shiqin He*, Jiaxing Zhao, Chunyue Wang and Hui Wang**

School of Civil Engineering, North China University of Technology, Beijing, 100144, China

*Corresponding Author: Shiqin He. Email: heshiqin@ncut.edu.cn

Received: 21 October 2019 Accepted: 10 November 2021

## ABSTRACT

In marine environments, the durability of reinforced concrete structures such as bridges, which suffer from the coupled effects of corrosion and fatigue damage, is significantly reduced. Fatigue loading can result in severe deterioration of the bonds between reinforcing steel bars and the surrounding concrete, particularly when reinforcing bars are corroded. Uniaxial tension testing was conducted under static loading and fatigue loading conditions to investigate the bonding characteristics between corroded reinforcing bars and concrete. An electrolyte corrosion technique was used to accelerate steel corrosion. The results show that the bond strength was reduced under fatigue loading, although the concrete did not crack. Therefore, fatigue loading has negative effects on the bond strength between corroded steel bars and concrete. The effects of corrosion cracking on bond strength become more pronounced after corrosion cracking appears along the main reinforcing bars. When the average width of cracking along main reinforcing bars exceeds 3 mm, the bonding properties deteriorate rapidly based on the effects of corrosion cracking, whereas fatigue loading exhibits no additional effects on bond strength.

## KEYWORDS

Reinforced concrete; fatigue loading; electrolyte corrosion; bond; uniaxial tension

## 1 Introduction

Marine environments are some of the most aggressive environments on earth. Corrosion damage to reinforced concrete (RC) structures is a significant problem that necessitates billions of dollars in repairs for highway structures every year [1]. Such damage is initiated and sustained by the chemical action of chlorides that are exposure to marine environments [2]. Damage to concrete structures, often resulting from the corrosion of reinforcing steel bars, is exhibited in the form of expansion, cracking, and spalling of the concrete covering such bars [3,4]. In addition to coverage loss, a RC member may also experience structural failure based on the failure of bonds between the concrete and steel [5]. Many marine concrete structures, such as floating structures, mobile drilling structures, offshore structures, and bridges are subjected to various types of fatigue cycles. In addition to corrosion, fatigue loading is a significant factor for determining the lifespan of a structure because it significantly accelerates the deterioration process in corrosive marine environments [6].

Because controlling crack width and deflection in RC members are the most important requirements for serviceability, considerable research has been devoted to understanding bonding, tension stiffening, and

crack width control. The study on the bond deterioration behavior between steel and concrete is usually carried out by beam experiment or pull-out test and finite element method. The majority of existing studies focus on the influence of corrosion or fatigue on the bond strength and bond stress-slip relation. Al-Sulaimani et al. [7] conducted investigations on the bond deterioration used pullout tests considering reinforcement diameter, corrosion rate and the cover to diameter ratio. It was found that the corrosion at the early stage has positive influence on bond strength, but afterwards the bond strength decreased consistently with increased corrosion level. Mangat et al. [8] found corresponding relationship between the bond strength and the degree of reinforcement corrosion under different levels of corrosion using beam specimens. This phenomenon was confirmed by many other scholars [9]. Lundgren [10] developed a model of three-dimensional finite element to analyse the bond tests of beams and pull-out tests with corroded reinforcement carried out by various researchers. The results were compared, and reasonably good agreement was found. Furthermore, the model was used to study the effect of uniform or localized corrosion. Fu et al. [11] studied the bond degradation of non-uniformly corroded steel rebars embedded in concrete using pull-out tests. Shang et al. [12] conducted beam-bonded tests under coupling of three different levels of sustained loads and chloride attack to study the bond properties between the rebar and concrete. Previous studies mainly focus on the monotonic bond behavior, while the bond deterioration under repeated loading has not been given sufficient attention. Several studies indicate that repeated loading results in progressive bond deterioration. Oh et al. [13] proposed a realistic model for bond stress-slip relation under repeated loading, and conducted a series of tests to explore the bond-slip behavior under repeated loadings. Zhang et al. [14] studied the influence of fatigue load on the bond behavior between rebar and concrete by pull-out tests, and established an empirical model of splitting failure for the bond stress-slip relationship of specimens under repeated loading, but the corrosion of rebar was not taken into consideration. Currently, investigations regarding the combined effects of repeated loading and steel corrosion on bond behavior is rare in the literature. Al-Hammoud et al. [15] and Lin et al. [16] have carried out investigations in this respect. Lin et al. [16] carried out a series of pull-out tests to investigate the bond deterioration due to the repeated loading of corroded reinforcement. A model for bond stress-slip relationship under repeated loading was proposed through systematic evaluation of the test data. Li et al. [17] conducted an experimental study on bolted connection steel plates, studied the combined effect of corrosion and fatigue on the fatigue strength of steel connection plates, and established a model for fatigue strength degradation as a function of corrosion rate. Wang et al. [18] studied the fatigue performance of reinforced concrete beams under coupled effects of the cyclic load and corrosive environment, but these tests did not involve the bond deterioration performance between the rebar and concrete.

Owing to the bond between reinforcing bars and surrounding concrete, the concrete between neighboring cracks can still carry tensile stress when cracking emerges in reinforced concrete members. This phenomenon known as the tension stiffening. Massicotte et al. [19] presented a simple incremental two-dimensional hypoelastic model for the description of tension stiffening in which two types of fixed crack model and two types of rotating crack model are considered. The model predictions were compared with the results of tests of reinforced concrete members in uniaxial tension. Khalfallah et al. [20] described the stress-strain relationship of the tension stiffening effect in the range of cracking to quantify the tension stiffening phenomenon in the cracking range. Shima et al. [21] built micro and macro models to understand the bond in reinforced concrete. Other studies have been carried out for tension stiffening in lightly reinforced concrete slabs, steel fiber-reinforced concrete, FRP reinforced concrete and recycled aggregate concrete [22–25]. Bui et al. [26] studied the tensile stiffening behavior by means of mesoscopic and macroscopic hydromechanical lattice simulations and proposed a feasible research method for the tensile stiffening of reinforced concrete.

However, relatively little effort has been devoted to evaluating the effects of corrosion on bonding behaviors and tension stiffening [27–29]. It is important to evaluate the load carrying capacity of existing concrete bridges that have been damaged by corrosion and fatigue to develop proper maintenance strategies, such as repair, strengthening, or reconstruction. However, the structural behavior of damaged beams has not been fully clarified in previous studies. In this study, tension specimens were fabricated and an electrolyte corrosion technique was used to accelerate steel corrosion. The bonding characteristics between the reinforcing bars after experiencing different degrees corrosion and the concrete under static loading and fatigue loading conditions were investigated.

## 2 Experimental Setup

### *2.1 Specimen Preparation*

Tension specimens with sizes of 100 × 100 × 1000 mm were reinforced with one reinforcing bar (20 mm in diameter and 1200 mm in length), as shown in Fig. 1. The concrete covering thickness was 40 mm. The average yield strength of the reinforcing bars was experimentally determined to be 337.5 MPa. The tensile strength was 515.9 MPa and the elastic modulus was $1.81 \times 10^5$ MPa. A water-to-cement ratio of 0.6 with no chloride additives was used for concrete fabrication. The average compressive strength of the resulting concrete cubes after 28 d of curing was 30 MPa. The final concrete specimens were cast in specifically designed wooden framework, as shown in Fig. 2, with sockets affixed to the left and right ends of the moulds to allow for the insertion of steel reinforcing bars and ensure uniform concrete covering thickness. The reinforcing bars extended 100 mm past each end of the concrete specimens. The protruding sections of the reinforcing bars and 20 mm sections on the ends of the specimens were coated with epoxy to prevent corrosion damage to these sections. The tension specimens were air cured in the wooden moulds for 28 d prior to being immersed in the exposure tank.

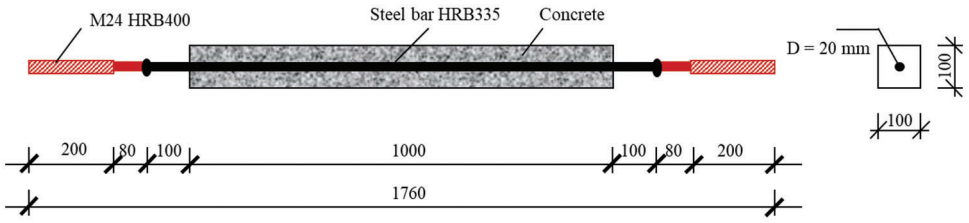


**Figure 1:** Tension specimen (unit: mm)

**Figure 2:** Designed wooden framework

### 2.2 Accelerated Corrosion Testing

After the tension specimens were cured for 28 d, a group of four specimens that were connected in parallel was submerged in a tank filled with an electrolytic solution (3.5 wt% NaCl solution). The solution level in the tank was adjusted to the midline of the specimens, as shown in Fig. 3.

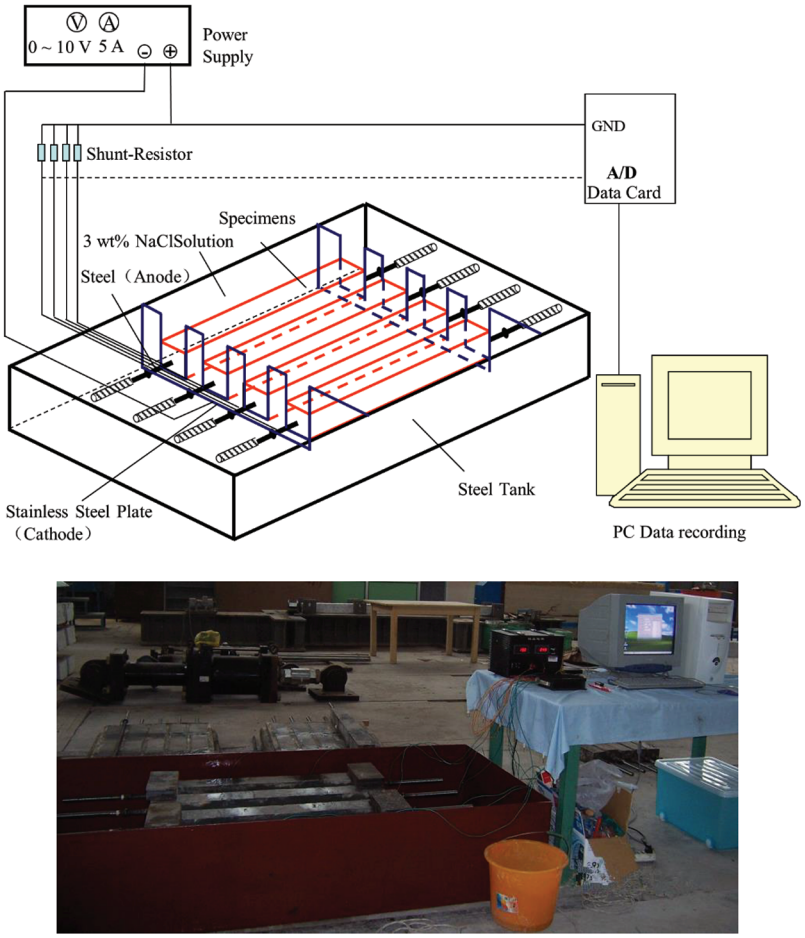


**Figure 3:** Accelerated corrosion setup

An external direct current was applied to the specimens through a DC power supply with a voltage limit of 10 V and maximum current output of 5 A to accelerate the corrosion process. One end of the rectifier was connected to the reinforcing steel bars in the specimens through a shunt-resistor and the other end was connected to a stainless steel plate that acted as a cathode for the accelerated corrosion process. The corrosion currents were recorded every 1800 s. Faraday's law determines the theoretical relationship between the time over which an induced current flows and the extent of corrosion. According to Faraday's law, the corrosion level (defined as weight loss or percentage weight loss of the reinforcing steel bars) can be calculated based on the current values measured by a PC, as shown in Fig. 3. The total weight loss of a reinforcing steel bar can be expressed as follows [30]:

$$W_{loss} = [TC] \cdot \frac{EW}{F} = \left\{ \sum_{j=1}^{n} \left[ \frac{I_j + I_{j-1}}{2} \right] \cdot (t_j - t_{j-1}) \right\} \cdot \frac{EW}{F} \tag{1}$$

where $W_{loss}$ is the total weight loss of the reinforcing steel bar in g, $TC$ is the total electric charge in A·s or C, and $EW$ is an equivalent weight indicating the mass of the oxidised metal in g. For pure metal elements, $EW$ is given by $EW = W/\mathrm{n}$, where $W$ is the atomic weight of the element and n is the valence of the element. For carbon steel, $EW$ is approximately 28 g. $F$ is Faraday's constant of electric charge ($F = 96490\,\mathrm{C}$ or $\mathrm{A{\cdot}s}$) and $I_j$ is the current in amps at time $t_j$ in s.

### *2.3 Fatigue and Static Tension Loading Testing*

The tension tests were performed using an MTS hydraulic servo-controlled universal testing machine with a capacity of 100 kN of tension. The specimens were tested under loading control. Axial loading was determined using the MTS data acquisition system and the strains at each deformation stage were determined by using displacement transducers (linear variable differential transformers) in the tops and bottoms of the specimens, as shown in Figs. 4 and 5. One set of specimens was subjected to static tensile loading until failure, theand anorther set of specimens was subjected to fatigue loading with a frequency of 1 Hz and Static then static loading failure occurred after 20,000 fatigue cycles. The static tensile cracking load Pcr was obtained from control specimen No. 19. The upper limit of the fatigue load was 0.8Pcr and the lower limit was 2.0 kN with a loading frequency of 1 Hz. The number of loading cycles was 20,000. After the fatigue loading tests, the specimens were subjected to static tensile loading up to the tension capacity of the machine. The cracks were then traced on the concrete surfaces and the corresponding load levels were recorded.

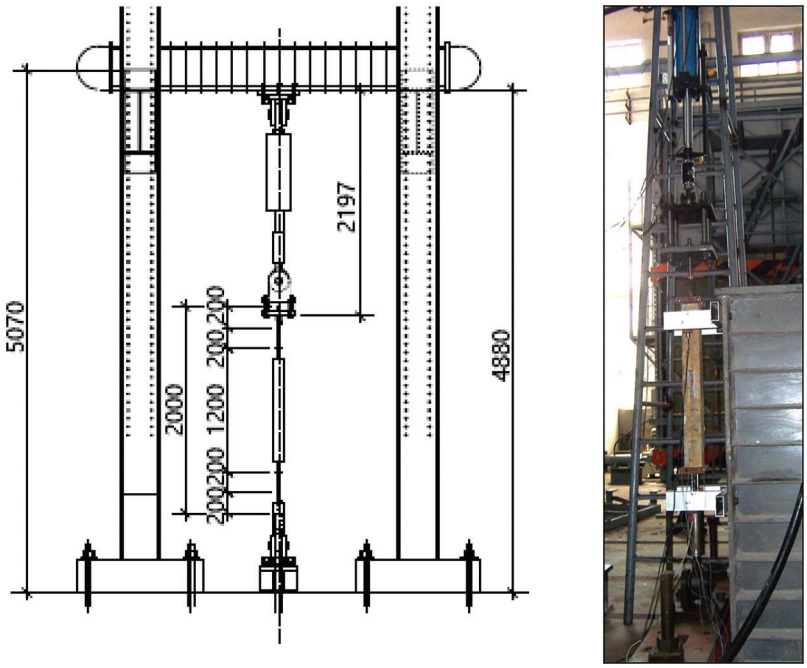


**Figure 4:** Loading test device diagram (unit: mm)

### *2.4 Quantification of the Extent of Corrosion*

Following the tension loading tests, the resulting crack patterns were recorded. The main tensile reinforcing bars were then carefully removed from the corroded specimens and cleaned of all adhered mortar and corrosion products, as shown in Fig. 6. The bars were then weighed to determine the extent of corrosion. For this process, the bars were dipped into a diluted HCl solution and then into an alkali

solution. After being washed with clean water, the bars were oven-dried and brushed with a brass bristle brush to remove all loosely adhered mortar and corrosion products. The corrosion level was determined by using the following gravimetric method [31]:

$$\rho_s = \frac{\omega_0 - \omega_\rho}{\omega_0} \times 100\% \tag{2}$$

where $\omega_0$ is the initial weight per unit length of the reinforcing bar prior to corrosion and $\omega_\rho$ is the final weight per unit length of the reinforcing bar after removing the corrosion products.

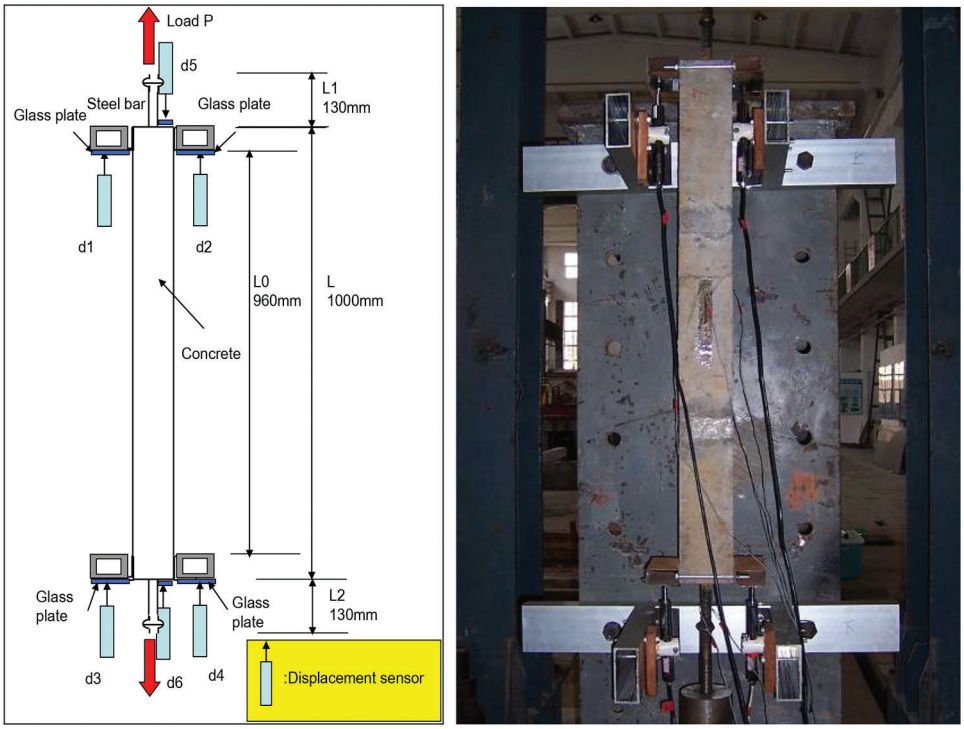


**Figure 5:** Displacement measuring method


**Figure 6:** Corroded steel bar removed from concrete

## 3 Results and Analysis

### *3.1 Tensile Force and Deformation Curve Calculation*

A cracked RC tension member has lower tensile stiffness than prior to cracking. However, within the tension zone of the tension member, intact concrete between adjacent cracks is still able to sustain a certain level of tensile stress and contribute to the tensile stiffness of the member [32,33]. This phenomenon is called tension stiffening because the tension member is apparently 'stiffened' by the tensile resistance of concrete, as shown in Fig. 7d. When a section cracks under an axial tensile force, the concrete no longer bears tension in the cracked section and the reinforcing bar takes on the tension from the concrete. This causes a sudden increase in the tensile stress on the reinforcing bar. The stress on the reinforcing bar $\sigma_s$ is maximised in the cracked section and decreases gradually with increasing distance from the cracked section. The stress is minimised between two different cracked sections. The strain distribution of the reinforcing bar is the same as the distribution of the stress $\sigma_s$, as shown in Fig. 7a. The tensile stress distribution of the concrete is opposite to that of the reinforcing bar. The stress of the concrete $\sigma_t = 0$ near cracked sections and is maximised between cracked sections. However, this stress does not exceed its tensile strength limit, as shown in Fig. 7e. Tensile stresses are induced in the concrete between cracks by stress transfer through the bond between the concrete and reinforcing bar. The bond between the concrete and reinforcing bar experiences local damage on both sides of a crack following a relative slip, but the bonds elsewhere remain strong.

Specimen elongation can be measured experimentally, as shown in Fig. 5. The average strain ε can then be calculated based on the elongation. From the calculated strain ε, the tensile force on a bare bar $P_s$ and tensile force on concrete $P_{con}$ are calculated according to the stress–strain relationship of the steel, as shown in Fig. 7b, and the stress–strain relationship of the concrete, as shown in Fig. 7f, respectively. Therefore, the axial force $P$ on an RC member can be obtained by using Eqs. (3)–(6):

$$\varepsilon = \frac{D_0}{L_0} \tag{3}$$

$$P_{s,m} = E_s \varepsilon A_s \tag{4}$$

$$P_{c,m} = \sigma_c (A - A_s) \tag{5}$$

$$P = P_{s,m} + P_{con} \tag{6}$$

where $D_0$ is specimen elongation, $L_0$ is specimen length, $P_{con}$ is tensile force on the concrete, $P_{s,m}$ is tensile force on a bare bar, $P_{s,m} + P_{con}$ is tensile force on the RC, $A$ is cross-sectional area of the specimen ($mm^2$), $A = 100 \times 100$ ($mm^2$), $A_s$ is cross-sectional area of the reinforcing bars after corrosion, $A_s = A_{s0}(1 - \rho_s)$, $A_{s0}$ is the initial cross-sectional area of the reinforcing bars and $\rho_s$ is the weight loss ratio of the reinforcing bars, $E_s$ is elastic modulus of the reinforcing bar, $E_c$ is elastic modulus of the concrete, $\sigma_c$ is concrete stress, $\varepsilon_t$ is cracking strain of concrete, $\varepsilon_t = \frac{P_{cr}}{E_c A_c + E_s A_s}$, where $P_{cr}$ can be obtained experimentally.

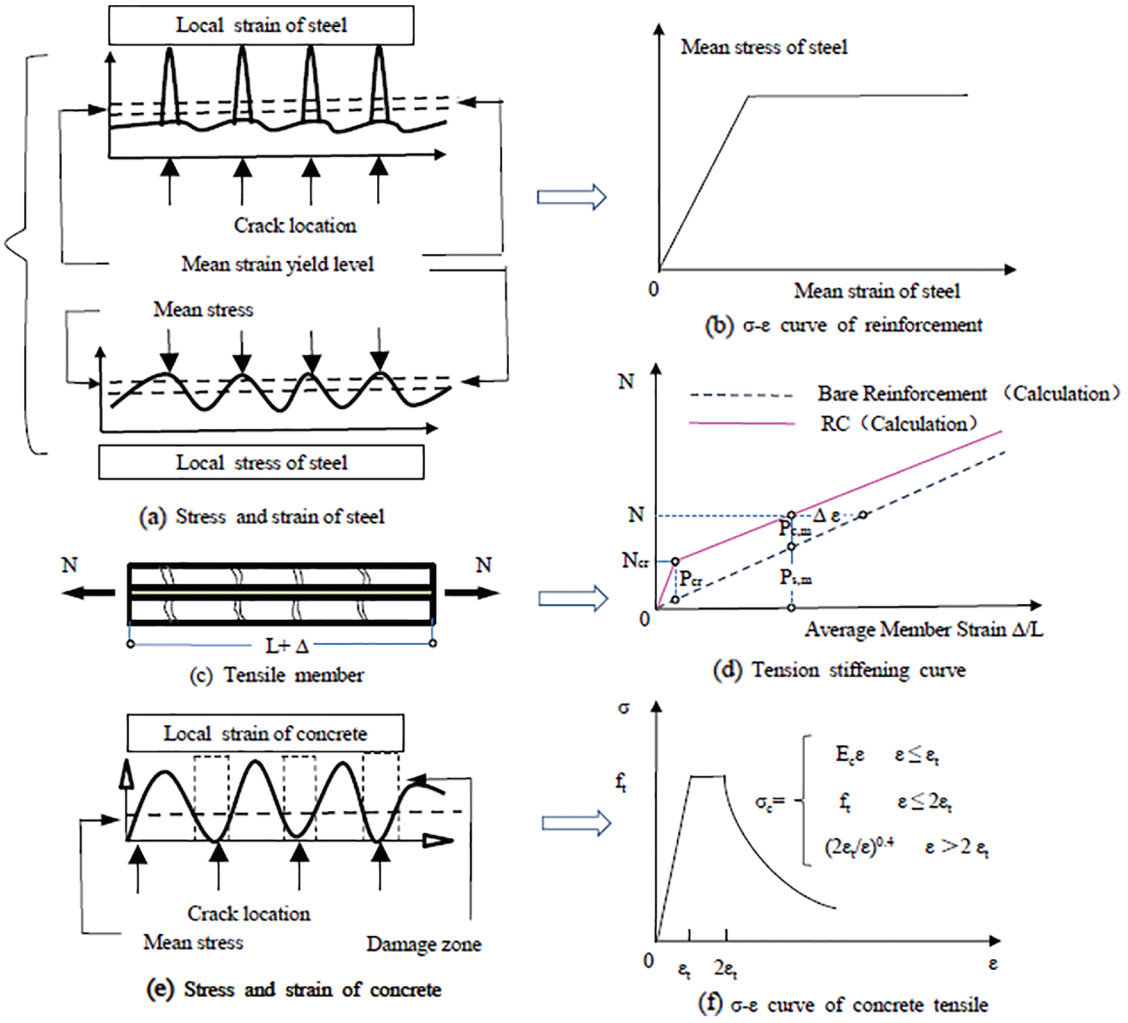


**Figure 7:** Tensile stiffness effects [34]
(a) Stress and strain of steel, (b) σ–ε curve of reinforcing bar, (c) tensile member, (d) tension stiffening curve, (e) stress and strain of concrete, and (f) σ–ε curve of concrete.

### *3.2 Degradation Ratio of Bonding*

As shown in Fig. 8, during the loading process for the uniaxial tensile tests on the RC members, some bond slip may occur between the loading ends of the steel bars and concrete. For the uncorroded specimens, the slip between the reinforcing bar and concrete is small and its influence on the load–deformation curve is generally negligible. However, when cracks along the reinforcing bar appear as a result of steel corrosion, the restraining and bonding effects of the concrete on the reinforcing decrease gradually and the bond stress at the steel–concrete interface is reduced, resulting in increased slippage between the steel bars and concrete at various locations. As slippage accumulates along the length of the bar towards the loading end, the measured RC member elongation is reduced for corroded members [35]. The degradation ratio $D_{\text{bond}}$ is calculated as follows:

$$D_{\text{bond}} = \frac{\delta_0 - \delta_1}{\delta_0} \times 100\% \tag{7}$$

where $\delta_0$ is the elongation of the control specimen and $\delta_1$ is the elongation of a specimen in which bond slip occurred.

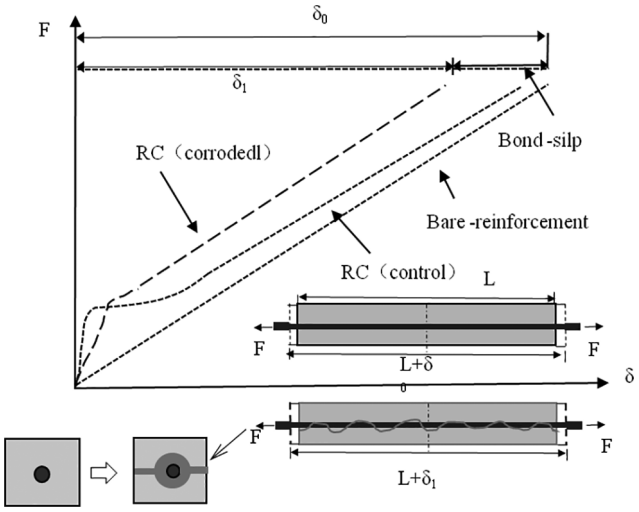


**Figure 8:** Bond degradation diagram

The load–elongation curve of control specimen No. 19 was calculated based on complete bonding between the steel bar and concrete. The calculated result agrees well with the experimental result. It was considered that bond slip did not occur because the bond between the reinforcing bar and concrete was maintained by an end load of 90 kN for specimen No. 19. Therefore, the load–elongation curve of specimen No. 19 was used as a control curve for comparison. The elongation of the specimens was obtained experimentally by displacement transducers. The elongation of the concrete is equal to that of the steel bar if the bond between the steel bar and concrete is maintained. When bond slip occurs between the concrete and reinforcing bar, the elongation of the concrete, which differs from that of the reinforcing bar, is smaller than that in the control specimen. The experimental results indicate that the bond between the steel bar and concrete deteriorates based on corrosion and fatigue loading. The bonding degradation ratios of the specimens are listed in Table 1.

**Table 1:** Experimental results

| Specimen | Corrosion time (h) | Corrosion level calculated (%) | Corrosion level gravimetric (%) | Corrosion cracking (mm) | Loading state | Concrete strength (MPa) | $D_{bond}$ (%) |
|---|---|---|---|---|---|---|---|
| No. 2 | 203.20 | 9.12 | 8.14 | no | static | 45.1 | 23.80% |
| No. 3 | 246.70 | 9.31 | 8.14 | 3.0–6.0 | fatigue | 43.0 | 35.50% |
| No. 4 | 246.70 | 7.84 | 7.34 | 3.0–5.0 | static | 43.5 | 36.40% |
| No. 9 | 178.80 | 9.05 | 8.04 | 0.75–6.0 | fatigue | 40.2 | 18.80% |
| No. 14 | 134.00 | 2.97 | 3.01 | 0.5–1.5 | fatigue | 38.6 | 16.40% |
| No. 15 | 134.00 | 2.95 | 2.54 | 0.3–0.75 | static | 37.4 | 12.40% |
| No. 16 | 0 | 0 | 0 | 0 | fatigue | 40.7 | 16.20% |
| No. 17 | 129.00 | 3.60 | 3.86 | 1.25–3.0 | static | 42.0 | 20.10% |
| No. 18 | 0 | 0 | 0 | 0 | fatigue | 45.3 | 19.50% |
| No. 19 | 0 | 0 | 0 | 0 | static | 45.3 | 0 |
| No. 20 | 129.00 | 3.47 | 2.76 | 0.5–1.5 | fatigue | 45.8 | 17.90% |

### *3.3 Bond Degradation in Uncorroded Specimens after Fatigue Loading*

Fig. 9 shows the load–elongation curves of specimen No. 16, which cracked under fatigue loading and specimen No. 18, which did not crack during the fatigue loading process. The degradation ratio is 16.2% for specimen No. 16 and 19.5% for specimen No. 18. The test results indicate that bonding at the steel–concrete interfaces deteriorated after 20,000 loading cycles. However, the concrete cracked during the process of fatigue loading for specimen No. 18. Fatigue loading had a noticeable effect on the bonds between the concrete and uncorroded reinforcing bars.

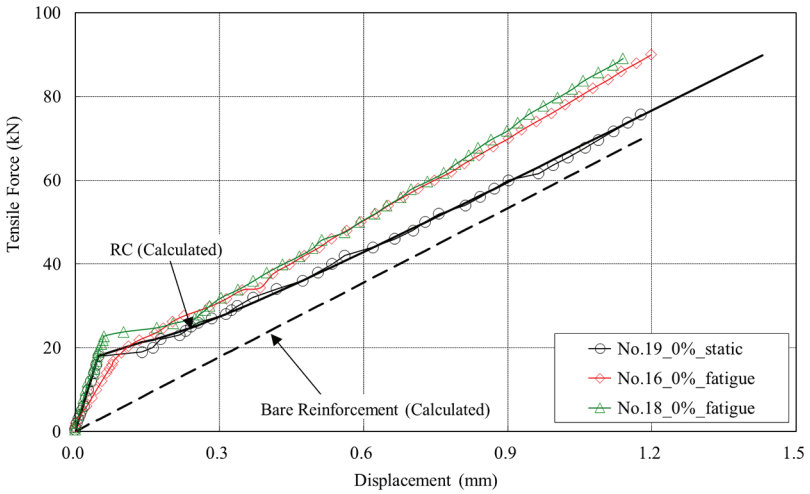


**Figure 9:** Tensile force-displacement curves for uncorroded specimens

### *3.4 Bond Degradation in Corroded Specimens*

As a result of corrosion, corrosion products accumulated along the peripheries of the steel bars. Based on the internal pressure created by the increased volume of the corrosion products, the tensile stresses in the concrete exceeded its tensile strength and generated the longitudinal cracks observed in all of the corroded specimens. Therefore, the adhesion between the concrete and reinforcing steel bars was partially lost before the specimens were tested. The load–elongation curves for the corroded specimens are shown in Fig. 10 with the responses of a bare reinforcing bar. The corrosion levels of specimens No. 14, No. 15, and No. 20 are 3.01%, 2.54%, and 2.76%, respectively, whereas the bond degradation ratios are 16.4%, 12.4%, and 17.9%, respectively. The test results clearly indicate that the strength of the bonds between the concrete and reinforcing steel deteriorated when the embedded reinforcing bars were corroded. The bond degradation ratio of specimen No. 15, which was subjected to static tensile loading, is smaller than that of specimens No. 14 and No. 20, which were subjected to fatigue loading. This indicates that fatigue loading has negative effects on bond strength at the steel–concrete interface. The corrosion cracking width was in the range of 0.3–0.75 mm for specimen No.15 and in the range of 0.5–1.5 mm for specimens No. 14 and No. 20. Therefore, the bond degradation of specimen No. 15 is less prominent than that of No. 14 and No. 20 based on its smaller longitudinal cracking width. The corrosion levels of specimens No. 2, No. 9, and No. 17 are 8.14%, 8.04%, and 3.86%, respectively. The corrosion cracking width is in the range of 1.0–6.0 mm for all three specimens. The bond degradation ratios are 23.8%, 18.8%, and 20.1%, respectively. The bond degradation of specimen No. 9, which was subjected to fatigue loading, did not exceed that of specimens No. 2 and No. 17, which were subjected to static loading. This indicates that the effects of fatigue loading on the bonds between reinforcing bars and concrete become less prominent with an increased width of longitudinal cracking. The other reason for the significant bond deterioration of specimen No. 2 is that longitudinal cracking appeared on two surfaces of this specimen.

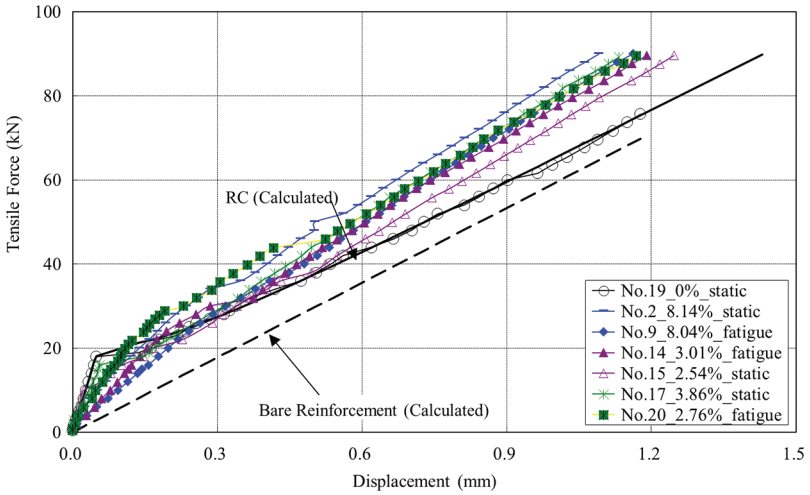


**Figure 10:** Tensile force-displacement curves for specimens subjected to static and fatigue loading with different levels of corrosion

### *3.5 Bond Degradation in Extensively Corroded Specimens*

As corrosion progresses, longitudinal cracking and the widening of cracks contribute to further loss of bond strength. The average corrosion crack widths for specimens No. 3 and No. 4 are much greater than 3 mm and their bond degradation ratios are 35.5% and 36.4%, respectively. Their load–elongation curves are shown in Fig. 11. The bond degradation ratio of specimen No. 3, which was subjected to fatigue loading, is the same as that of specimen No. 4. These results indicate that fatigue loading has no significant effects on the bond strength of extensively corroded specimens because the main reason for the loss of bond strength is the widening of cracks. Corrosion of reinforcing bar ribs has a significant influence on the mechanical interlocking between the steel bars and concrete, leading to a deterioration of bond strength between the corroded ribs on the surface of the steel bar and the concrete. Therefore, force is not transferred as efficiently from the steel bar to the concrete, leading to greater spacing between cracks in a specimen with a corroded bar compared to a specimen with an uncorroded bar. Crack spacing becomes very large in specimens with significant loss of bond strength. For example, specimens No. 3 and No. 4 did not exhibit any transverse cracking until they were loaded beyond the yield strength of the reinforcing steel bars, as shown in Fig. 11.

### *3.6 Analysis of Crack Formation*

The transverse and longitudinal cracks on all four surfaces of the members were traced after testing. Fig. 12 was the photos of cracks on four sides of specimen No. 9 after testing. The transverse load cracks and longitudinal corrosion cracks of the specimens were drawn according to the cracks in the photo, as shown in Figs. 13 and 14, which show the crack patterns for the tension specimens that were subjected to different levels of corrosion and loading in the experiments, the height of each of the four expanded surfaces in Figs. 13 and 14 is 100 mm. The numbers beside the transverse cracks represent the load levels at which the cracks appeared in kN. The longitudinal cracks (red lines) are corrosive cracks and the corresponding numbers represent crack widths in mm.

Several cracks with approximately equal spacing tended to appear after the RC members cracked for the uncorroded specimens, as shown in Fig. 13. From the concrete cracking distribution of the control specimen No. 19–0%-Static, one can see that there are six transverse cracks with a uniform distribution. Specimens No. 18–0%-Fatigue and No. 16–0%-Fatigue experienced static destruction after 20,000 fatigue loading

cycles with uncorroded reinforcing bars. Transverse cracking did not occur during the fatigue test for specimen No. 18, whereas specimen No. 16 experienced cracking after 10,000 fatigue loading cycles. There are five transverse cracks with a uniform distribution on specimen No. 18 and six transverse cracks including one fatigue-induced crack on specimen No. 16. There are fewer cracks with larger spacing on specimen No. 18 compared to specimen No. 19. Therefore, one can conclude that the effects of fatigue loading on the loss of bond strength result in a reduction of the rate at which force is transferred from the reinforcing bar to the surrounding concrete.

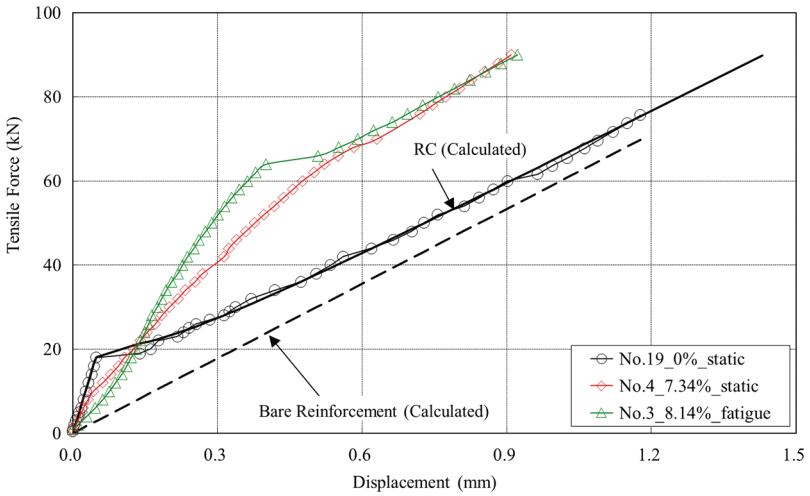


**Figure 11:** Tensile force-displacement curves for specimens No. 3, No. 4 and No. 19

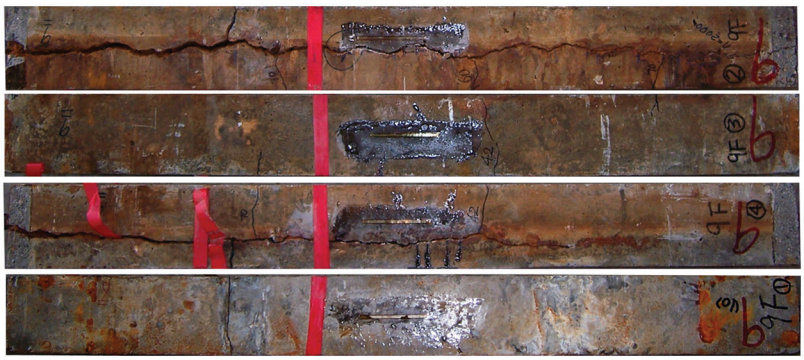

**Figure 12:** Cracks photos of specimen No. 9

The results for corroded specimens are compared to the crack pattern for the uncorroded specimen No. 19, as shown in Fig. 14. These comparisons clearly reveal the influence of corrosion. As the level of corrosion increases, the number of cracks decreases and crack spacing increased, indicating a decrease in the bond strength between the corroded steel and concrete. For specimens No. 14 and No. 15, which have average corrosion crack widths of less than 1 mm, the average number of transverse cracks is in the range of 4–5. The transverse cracking distributions are non-uniform compared to the uncorroded specimen and are nearly the same for specimen No. 15, which was subjected to static tensile loading and specimen No. 14, which experienced static loading failure after 20,000 fatigue loading cycles. This indicates that the decrease in bond strength is largely caused by the corrosion of reinforcing bars. For

specimens No. 17 and No. 20, which have average corrosion crack widths of 1.5 mm, three transverse cracks appeared in addition to the longitudinal cracks. The number of cracks decreased and the crack spacing increased compared to the previous specimens, indicating that bond strength was reduced further. Transverse cracking occurred on specimen No. 20 after 15,000 fatigue loading cycles. However, the number of cracks and their distributions are nearly the same as those on specimen No. 17, which was subjected to static tensile loading. This indicates that fatigue damage has little effect on bond strength reduction after corrosion cracking occurs. For specimens No. 2, No. 9, No. 3, and No. 4, which exhibited longitudinal corrosion cracking on multiple surfaces with an average corrosion crack width greater than 3 mm, one can conclude that the bond strength at the steel–concrete interface decreased significantly because only three transverse cracks occurred with very large crack spacing. Based on this reduced bond strength, the load on these specimens was largely carried by the steel reinforcing bars. The concrete carried a relatively small load compared to the uncorroded specimens. The maximum crack widths on the corroded specimens were much larger than those on the uncorroded specimens because of weaker bonding between the concrete and reinforcing bars.

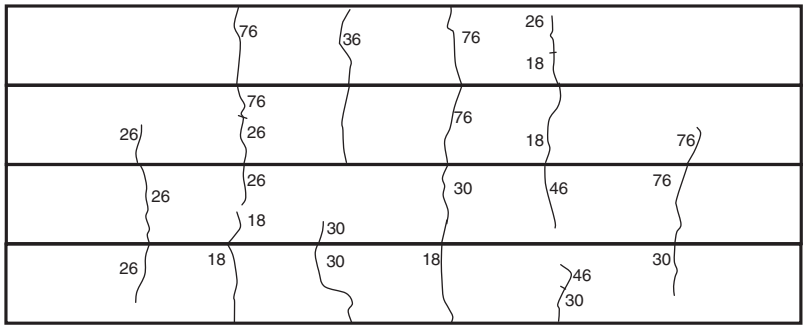


No. 19-0%-Static

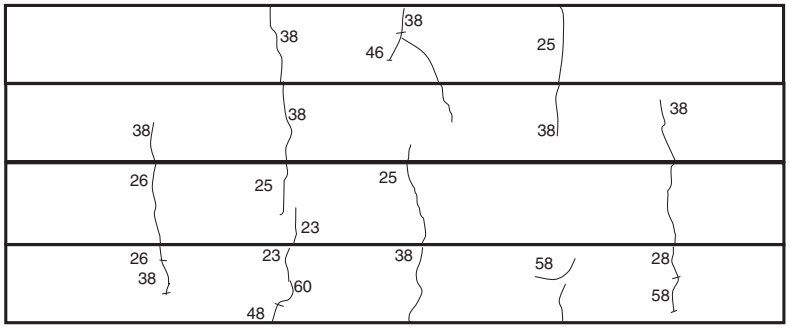


No. 18-0%-Fatigue

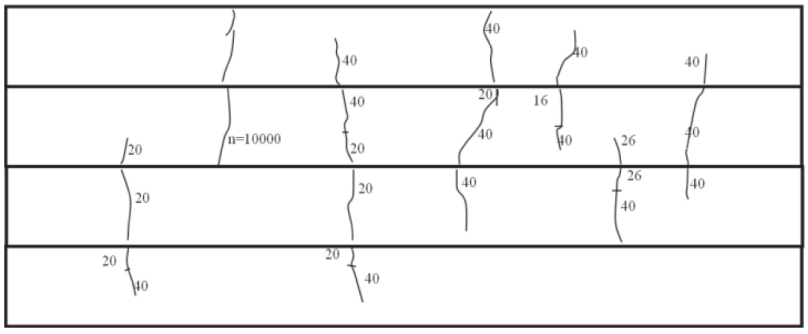


No. 16-0%-Fatigue

**Figure 13:** Transverse cracks on uncorroded specimens

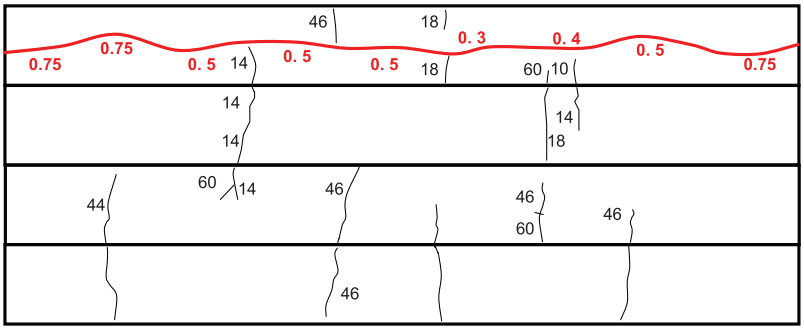


No. 14-3.01%-Fatigue

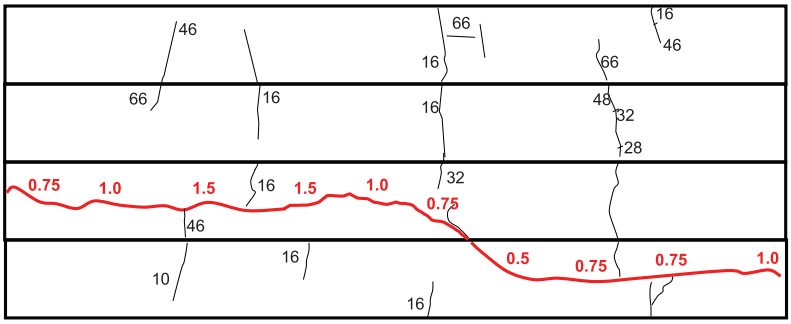


No. 15-2.54%-Static

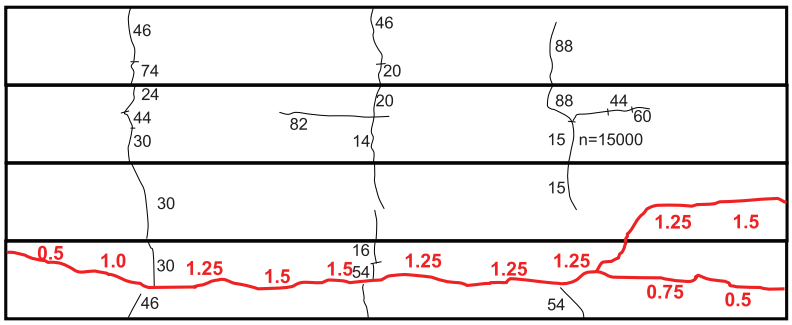


No. 17-3.86%-Fatigue

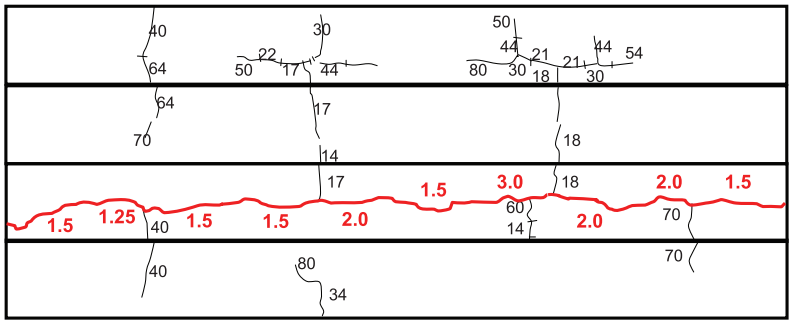


No. 20-2.76%-Fatigue

**Figure 14:** (Continued)


No. 2-8.14%-Static

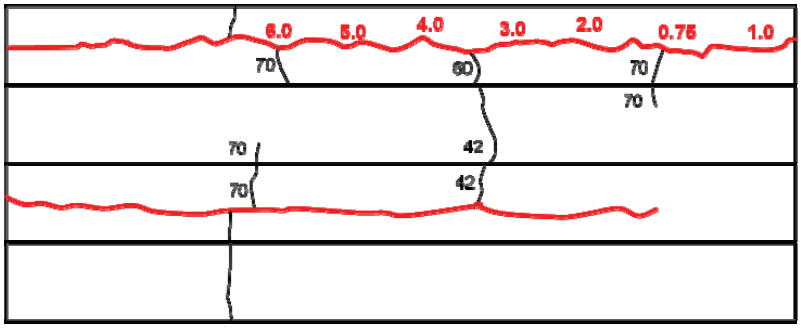


No. 9-8.04%-Fatigue

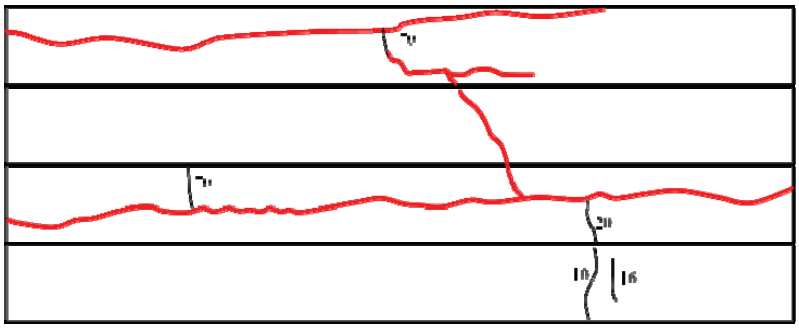

No. 3-8.14%-Fatigue

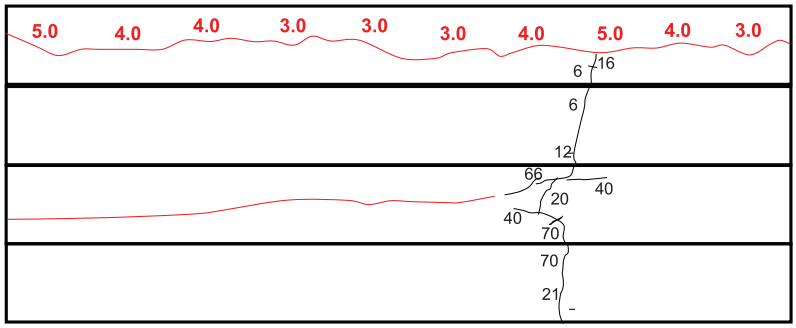


No. 4-7.34%-Static

**Figure 14:** Transverse and longitudinal cracking with different levels of corrosion

## 4 Conclusion

(1) The bond strength of uncorroded RC members was reduced by fatigue loading, but the concrete did not crack during loading. The number of cracks decreases and crack spacing increases based on the deterioration of bond strength between steel and concrete following fatigue damage.

(2) Fatigue loading has negative effects on the bond strength between corroded steel bars and concrete. The effects of corrosion cracking on bond strength become more prominent after corrosion cracking occurs along the main reinforcing bar. The number of cracks decreases and crack spacing increases to create a non-uniform transverse cracking distribution on specimens with corroded members.

(3) When the average width of cracking along the main reinforcing bar is greater than 3 mm, bond strength deteriorates significantly based on corrosion cracking, and fatigue loading has a negligible effect on bond strength. Extensively corroded members did not exhibit any transverse cracking until they were loaded beyond the yield strength of the reinforcing steel bars.

**Acknowledgement:** This work was supported by the Fundamental Research Funds for Beijing Universities (110052971921/059).

**Funding Statement:** This work was supported by the Fundamental Research Funds for Beijing Universities (110052971921/059). S H received the Grant. The fund is set up by the project unit itself so there is no URLs to sponsors' websites.

**Conflicts of Interest:** The authors declare that they have no conflicts of interest to report regarding the present study.

## References

1. Roberge, P. R. (2000). *Handbook of corrosion engineering*. New York: McGraw-Hill.
2. Broomfield, J. (1997). *Corrosion of steel in concrete*. London: E & FN Spon.
3. Metha, P. K., Gerwick, B. C. (1982). Cracking-corrosion interaction in concrete exposed to marine environment. *Concrete International, 10,* 45–51.
4. Bhargava, K., Ghosh, A. K., Morii, Y., Ramanujam, S. (2005). Modelling time to corrosion induced cracking in reinforcement concrete structures. *Cement Concrete Research, 35(11),* 2203–2215. DOI 10.1016/j.cemconres.2005.06.007.
5. Lundgren, K. (2007). Effect of corrosion on bond between steel and concrete: An overview. *Magazine of Concrete Research, 59(6),* 447–461.
6. Ahn, W., Reddy, D. V. (2001). Galvanostatic testing for the durability of marine concrete under fatigue loading. *Cement and Concrete Research, 31,* 343–349. DOI 10.1016/S0008-8846(00)00506-8.
7. Al-Sulaimani, G. L., Kaleemullah, M., Basunbul, I. A., Rasheeduzzafar. (1990). Influence of corrosion and cracking on bond behavior and strength of reinforced concrete members. *ACI Structural Journal, 87(2),* 230–231.
8. Mangat, P. S., Elgarf, M. S. (1999). Bond characteristics of corroding reinforcement in concrete beams. *Materials and Structures, 32(216),* 89–97. DOI 10.1007/BF02479434.
9. Auyeung, Y. B., Balaguru, P., Chung, L. (2000). Bond behavior of corroded reinforcement bars. *ACI Materials Journal, 97(2),* 214–220. DOI 10.1016/j.cemconres.2006.05.008.
10. Lundgren, K. (2005). Bond between ribbed bars and concrete. Part 2: The effect of corrosion. *Magazine of Concrete Research, 57(7),* 383–395. DOI 10.1680/macr.2005.57.7.383.
11. Fu, C. Q., Fang, D. M., Ye, H. L., Huang, L., Wang, J. D. (2021). Bond degradation of non-uniformly corroded steel rebars in concrete. *Engineering Structures, 226,* 111392. DOI 10.1016/j.engstruct.2020.111392.
12. Shang, H. S., Zhou, J. H., Fan, G. X., Yang, G. T., You, W. J. (2021). Study on the bond behavior of steel bars embedded in concrete under the coupling of sustained loads and chloride ion erosion. *Construction and Building Materials, 276,* 121684. DOI 10.1016/j.conbuildmat.2020.121684.

13. Oh, B. H., Kim, S. H. (2007). Realistic models for local bond stress-slip of reinforced concrete under repeated loading. *Structural Engineering, 133(2),* 216–224. DOI 10.1061/(ASCE)0733-9445(2007)133:2(216).
14. Zhang, W. P., Zhang, Y. P., Li, H., Gu, X. L. (2020). Experimental investigation of fatigue bond behavior between deformed steel bar and concrete. *Cement and Concrete Composites, 108,* 103515. DOI 10.1016/j.cemconcomp.2020.103515.
15. Al-Hammoud, R., Soudki, K., Topper, T. H. (2010). Bond analysis of corroded reinforced concrete beams under monotonic and fatigue loads. *Cement & Concrete Composites, 32,* 194–203. DOI 10.1016/j.cemconcomp.2009.12.001.
16. Lin, H. W., Zhao, Y. X., OžBolt, J., Hans-Wolf, R. (2017). The bond behavior between concrete and corroded steel bar under repeated loading. *Engineering Structures, 140,* 390–405. DOI 10.1016/j.engstruct.2017.02.067.
17. Li, L., Li, Y. R., Shi, W. H., Li, C. Q. (2021). Deterioration of fatigue strength of bolted connection plates under combined corrosion and fatigue. *Journal of Constructional Steel Research, 179,* 106559. DOI 10.1016/J.JCSR.2021.106559.
18. Wang, H., He, S. Q., Yin, X. Q., Cao, Z. Y. (2020). Experimental study on fatigue performance of reinforced concrete beams in corrosive environment with cyclic loads. *Structural Durability & Health Monitoring, 14(2),* 95–108. DOI 10.32604/sdhm.2020.06595.
19. Massicotte, B., Elwi, A. E., MacGregor, J. G. (1990). Tension-stiffening model for planar reinforced concrete members. *Journal of Structural Engineering, 116(11),* 3039–3058. DOI 10.1061/(ASCE)0733-9445(1990)116:11(3039).
20. Khalfallah, S., Guerdouh, D. (2014). Tension stiffening approach in concrete of tensioned members. *International Journal of Advanced Structural Engineering, 6,* 3–6.
21. Shima, H., Chou, L., Okamura, H. (1987). Micro and macro models for bond behavior in reinforced concrete. *Faculty Engineering, 39(2),* 133–194.
22. Gilbert, R. I. (2007). Tension stiffening in lightly reinforced concrete slabs. *Journal of Structural Engineering, 133(6),* 899–903. DOI 10.1061/(ASCE)0733-9445(2007)133:6(899).
23. Bischoff, P. H. (2003). Tension stiffening and cracking of steel fiber-reinforced concrete. *Journal of Materials in Civil Engineering, 15(2),* 174–182. DOI 10.1061/(ASCE)0899-1561(2003)15:2(174).
24. Baena, M., Torres, L., Turon, A., Miàs, C. (2013). Analysis of cracking behaviour and tension stiffening in FRP reinforced concrete tensile elements. *Composites Part B: Engineering, 45,* 1360–1367. DOI 10.1016/j.compositesb.2012.07.026.
25. Rangel, C. S., Amario, M., Pepe, M., Yao, Y. M., Mobasher, B. et al. (2017). Tension stiffening approach for interface characterization in recycled aggregate concrete. *Cement and Concrete Composites, 82,* 176–189. DOI 10.1016/j.cemconcomp.2017.06.009.
26. Bui, T. S., Pham, D. T., Vu, M. N., Nguyen, T. N., Nguyen-Sy, T. (2021). Modeling of the tension stiffening behavior and the water permeability change of steel bar reinforcing concrete using mesoscopic and macroscopic hydro-mechanical lattice model. *Construction and Building Materials, 291,* 123266. DOI 10.1016/j.conbuildmat.2021.123266.
27. Amleh, L., Mirza, S. (1999). Corrosion influence on bond between steel and concrete. *ACI Structural Journal, 96(3),* 415–423.
28. An, X. H., Shang, F., Shionaga, R., Maekawa, K. (2009). Residual seismic assessment of existing RC structures subjected to coupled corrosion and fatigue loading. *Proceedings of the First International Conference on Computational Technologies in Concrete Structures*, pp. 259–273. Jeju, Korea.
29. Kim, H., Choi, W., Yoon, S., Takafumi, N. (2016). Evaluation of bond properties of reinforced concrete with corroded reinforcement by uniaxial tension testing. *International Journal of Concrete Structures and Materials, 10(3),* 43–52. DOI 10.1007/s40069-016-0152-9.
30. ASTM (1989). Standard practice for calculation rates and related information from electrochemical measurement. *ASTM G, 102(89),* 400–406.
31. Ministry of Communications of People's Republic of China (1998). Testing code of concrete for port and waterway engineering JTJ270–98. Peoples Communication Press.

32. Nga, P. L., Lamb, J. Y. K., Kwan, A. K. H. (1953). Effects of concrete-to-reinforcement bond and loading conditions on tension stiffening. *Procedia Engineering, 14(11),* 704–714. DOI 10.1016/j.proeng.2011.07.090.
33. Gilbert, R. I. (2013). Time-dependent stiffness of cracked reinforced and composite concrete slabs. *Procedia Engineering, 57,* 19–34. DOI 10.1016/j.proeng.2013.04.006.
34. Maekawa, K., Pimanmas, A., Okamura, H. (2003). *Nonlinear mechanics of reinforced concrete*. London: Spon Press.
35. Shang, F., An, X. H., Kawai, S., Mishima, T. (2010). Open-slip coupled model for simulating three-dimensional bond behavior of reinforcing bar in concrete. *Computers and Concrete, 75(5),* 859–865.